npj | precision oncology

Article

Published in partnership with The Hormel Institute, University of Minnesota

https://doi.org/10.1038/s41698-025-01053-x

Molecular subtyping of endometrial carcinoma cell lines uncovers subtype-specific targetable vulnerabilities

Eunice S. Li[1,2,8], Rebecca Ho[1,2,8], Ran Tao[1,2], Yannes Wai Yan Choi[1,2], Chae Young Shin[1,3], Shary Y. Chen[1,2,3], Bengul Gokbayrak[1,2,3], Janine Senz[1,3], Betty Yao[1,4], Liam Johnston[1,4], Spencer D. Martin[1], Eric Yang[1], Mark S. Carey[5], Bryan T. Hennessy[6], David G. Huntsman[1,2,3,5], Ramon I. Klein Geltink[1,3,4,7], Lynn Hoang[1,2] & Yemin Wang[1,2,3] ✉

Endometrial carcinoma (EC), the most common gynecologic cancer type in developed countries, encompasses four molecular subtypes (*POLEmut*, MMRd, p53abn, and NSMP) that have prognostic values and guide treatment decisions. Additionally, dual loss of ARID1A and ARID1B (referred to as ARID1A/B) characterizes a significant portion of dedifferentiated/undifferentiated EC (DD/UDEC), a rare but highly aggressive subtype of EC. To advance the translational research for ECs, we analyzed the genomic features of a panel of 39 EC cell lines, leading to the identification of cell lines representing each of these EC molecular subtype. Histologic and immunohistochemical analyses of xenografted tumors from these cell lines confirmed their resemblance of cognate primary EC molecular subtypes. Further investigation of the publicly available genome-wide CRISPR screen data for EC cell lines identified multiple specific genetic dependencies in MMRd, p53abn, and ARID1A/B-dual deficient EC cell lines. Particularly, ARID1A/B-dual deficient DD/UDEC cells selectively rely on mitochondrial oxidative phosphorylation in vitro and in vivo. Therefore, through molecular subtyping of EC cell lines and subsequent characterization of molecular subtype-specific genetic dependencies, our study provides a framework that guides the utility of the EC cell line models for accelerating translational research in EC.

Endometrial carcinoma (EC) is the most common form of gynecologic cancer in developed countries, with increased incidence and mortality rates globally. While it can be grouped into two types, an estrogen-dependent type I that pertains to the majority of EC and a more aggressive estrogen-independent type II EC[1], the inconsistency of pathologic categorization often results in poor risk stratification for treatment. To overcome this challenge, the Cancer Genome Atlas (TCGA) and others have characterized the genomic landscape of ECs for molecular classification. Mismatch repair (MMR) deficiency and mutations of *PTEN, ARID1A, PIK3CA, CTNNB1, TP53*, and *POLE* genes occur frequently in EC[2,3]. Based on their gene mutation pattern and frequency, copy number variation, and microsatellite stability, TCGA classified common ECs into four distinct molecular subtypes: POLE ultra-mutated, microsatellite instable (MSI)/hypermutated, copy-number low, and copy-number high[2,4]. These molecularly defined groups are associated with distinct prognoses[2,4].

Building on TCGA's genomic analyses, novel clinically applicable molecular genotyping strategies, such as the ProMisE classifier[5,6] and the ESGO/ESTRO/ESP guideline[7], have been recently developed to stratify patients by risk into molecular subtypes. According to the ProMisE classification tree, EC can be classified into *POLE*-mutant, MMR-deficient (MMRd), p53-abnormal (p53abn), and no specific molecular phenotype (NSMP, lacking all prior three features) molecular subtypes. The hierarchy of classification that the ProMisE tree provides has been further supported by a recent study, in which p53 abnormal ECs with either MMR defect or

[1]Department of Pathology and Laboratory Medicine, University of British Columbia, Vancouver, BC, Canada. [2]Ovarian Cancer Research Centre, Vancouver Coastal Health Research Institute, Vancouver, BC, Canada. [3]Department of Basic and Translational Research, British Columbia Cancer Research Institute, Vancouver, BC, Canada. [4]BC Children's Hospital Research Institute, Vancouver, BC, Canada. [5]Department of Obstetrics and Gynecology, University of British Columbia, Vancouver, BC, Canada. [6]Royal College of Surgeons in Ireland, Dublin, Ireland. [7]Edwin S.H. Leong Centre for Healthy Aging, University of British Columbia, Vancouver, BC, Canada. [8]These authors contributed equally: Eunice S. Li, Rebecca Ho. ✉e-mail: yemin.wang@ubc.ca

POLE mutations are best classified under MMRd or *POLE*-mutant subtypes, respectively[8]. The prognosis of *POLE*-mutant subtype is excellent in contrast to the p53abn subtype, which has the most unfavorable outcome with a 5-year overall survival of ~40%, highlighting the need for effective treatments[9]. Both MMRd and NSMP subtypes have intermediate prognoses[5,6], but advanced and recurrent MMRd ECs often benefit from immune therapies, which is changing the outcome of this subtype[10,11]. Notably, some MMRd and NSMP ECs can dedifferentiate and progress to highly aggressive dedifferentiated or undifferentiated EC (DD/UDEC), diseases that lack biology-informed effective treatments.

DD/UDEC is often diagnosed at the peak age of 55 years. DDEC occurs when an undifferentiated carcinoma arises clonally from low-grade[12–14] or sometimes high-grade[15,16] endometrioid EC that are often MMR-deficient. The differentiated component is eclipsed in about 40% cases, likely due to an outgrowth of the undifferentiated component, and the tumor overall appears as a pure UDEC[12,17]. The endometrioid components, generally low-grade, often express estrogen receptor (ER), progesterone receptor (PR), and PAX8, whereas the undifferentiated components are usually negative with occasional focal positivity for ER and PAX8. Recent studies identified frequent inactivating mutations with protein loss in the members of the SWI/SNF chromatin-remodeling complexes, such as *SMARCA4* (encoding a core ATPase of all types of SWI/SNF), *ARID1B* (encoding a scaffold protein alternate to ARID1A in canonical BAF-type of SWI/SNF), and *SMARCB1* (encoding a core member of canonical BAF and PBAF-types of SWI/SNF) in the undifferentiated components of DD/UDEC[18–21]. Furthermore, SMARCA4 inactivation is accompanied by the protein loss of SMARCA2, the only known alternate ATPase; and the inactivation of ARID1B occurs along with ARID1A genetic inactivation, in which ARID1A inactivation is usually present in both differentiated and undifferentiated components of DDEC. These findings suggest that inactivation of canonical BAF-type SWI/SNF complexes is one major driving force underlying the development of DDEC/UDEC. Additionally, these SWI/SNF-mutant DD/UDECs are typically associated with an extremely poor outcome[22,23], thus demanding novel, effective treatments.

Cancer cell lines established from human tumor specimens remain the most commonly used models in cancer research. There are dozens of EC cell lines that were established and reported over the past several decades. However, the lack of genomic profiles for most EC cell lines at the time of their establishment posed a barrier for proper pathological and molecular classification. The Broad-Novartis Cancer Cell Line Encyclopedia (CCLE) project has profiled the genomic features of about 1000 cancer cell lines of most common cancer types and centralized the data in the DepMap database at the Broad Institute. This study molecularly stratifies all EC cell lines in this database, complemented by the in-house analysis of additional EC cell lines to aid in molecular subtype-specific cancer research. Based on this molecular classification framework, we further analyzed the DepMap genome-wide CRISPR knockout screen database and uncovered molecular subtype-specific lethal targets for future therapeutic development.

Results

Molecular subtyping of EC cell lines

To correlate the genomic features of EC cell lines with EC molecular subtypes, we determined the mutation statuses of *POLE*, mismatch repair genes and *TP53* in 39 EC cell lines using the exome-sequencing data (32 from DepMap, 3 sequenced in-house), cancer gene panel sequencing (2 sequenced in-house), and the microsatellite stability information (Cell Model Passports database) (Fig. 1a). Two cell lines, HEC251 and JHUEM7, harbor pathogenic *POLE* mutations and 23 have microsatellite instability and/or mutant mismatch repair genes, including AN3CA, COLO704, EN, HEC1 (HEC1A, HEC1B), HEC108, HEC116, HEC151, HEC265, HEC59, HEC6, HHUA, HOUA-I, ISHIKAWA, JHUEM1, MFE296, MFE319, RL962, SNGM, VOA12371, and VOA14590H (Fig. 1b, Supplementary Table S1). For the remaining 14 cell lines, 12 have p53 pathogenic mutations and one (VOA8492) has a homozygous deletion at p53 loci (Fig. 1b). Immunoblotting validated aberrant p53 expression in all 7 out of 13 p53abn cell lines available for testing, including protein loss in TEN, VOA8492, VOA14581 and HEC50B cells and dominant-negative mutant expression in KLE, EFE184 and SPAC1L cells (Fig. 1c, Supplementary Fig. S1). Therefore, our analysis identified all four molecular subtypes of ECs, including 5.2% (2/39), 59% (23/39), 33.3% (13/39), and 2.6% (1/39) for *POLEmut*, MMRd, p53abn, and NSMP, respectively. The tumor mutational burden (TMB) correlates well with the molecular classification, ranging from 180 to 200 in two *POLEmut* cell lines, 10–132 in MMRd cell lines, 1–20 in p53abn cell lines, and 7.5 in the NSMP cell line (VOA1066). The mutation burden of MMRd EC cell lines is significantly higher than that in p53abn EC cell lines (Fig. 1d, $p < 0.0001$).

P53abn EC cell lines share common genomic features with their primary tumors

As p53abn EC represents the most lethal of the four molecularly defined EC molecular subtypes, we sought to address whether the identified p53abn EC cell lines recapitulate the genomic features of primary tumors of p53abn EC. Among the 60 cases of copy number-high ECs from the TCGA where nearly all were p53abn (Fig. 2a)[2], somatic nucleotide variants of *PIK3CA, FBXW7, PPP2R1A, PIK3R1, ARHGAP35* and *PTEN* were present in 47%, 22%, 22%, 13%, 12% and 10% of samples (Supplementary Data 1), respectively. Moreover, amplification of multiple cancer genes were found in >15% of samples (Fig. 2a, Supplementary Data 2), including those at genomic loci 3q25-29 (15-36.7%: *TERC, MECOM, PIK3CA, SOX2*), 17q12 (*ERBB2* and *GRB7*, 25%), 8q24.21 (*MYC*, 23.3%), 19p13 (*NOTCH3, BRD4, SMARCA4, KEAP1*, 20-26.7%), 19q12 (*CCNE1*, 23.3%), 1q21-22 (*MCL1*, 20%; *MUC1*, 23.3%), 8p11.21 (*KAT6A*, 18.7%), 20q13 (*ZNF217*, 16.7%), 20q11 (*ASXL1*, 21.7%), 16p11.2 (*SETD1A*, 16.7%), 5p13.3 (*DROSHA*, 15%), and 2p23 (*PPP1CB*, 15%). These findings are largely recapitulated in our recent targeted cancer gene mutation analysis and shallow whole genome sequencing of 186 p53abn EC primary tumors[24]. Based on these genomic features, about 75% of p53abn ECs contain one or more of the four following targetable features: *ERBB2* amplification, *CCNE1* amplification, *PPP2R1A/FBXW7* mutations, and homologous recombination deficiency[24].

Among all 13 p53abn EC cell lines, two (HTMMT, SPAC1L) have inactivating *PTEN* and two (TEN and MFE280) have activating *PIK3CA* mutations (Fig. 2b). Three cell lines, including TEN, MFE280 and VOA8492, have amplification of *ERBB2* (Fig. 2c). *MYC* is amplified at least 1.5-fold in 4 cell lines, including SNU685, VOA14581, JHUEM3 and SNU1077 cells (Fig. 2c). Remarkably, *CCNE1* is amplified at least 1.5-fold in 7 seven cell lines, including TEN, EMTOKA, KLE, VOA14581, MFE280, VOA8492 and SNU1077 (Fig. 2c). Western blotting analysis confirmed elevated CCNE1 expression in four *CCNE1*-amplified cell lines, including TEN, KLE, VOA14581 and VOA8492, in comparison to HEC50B and VOA1066, two cell lines with normal *CCNE1* copy numbers (Fig. 2d, Supplementary Fig. S2). Notably, SPAC1L also expressed abundant CCNE1 despite of no *CCNE1* amplification, which may be due to a hotspot mutation (p.R505S) in WD40 domains of FBXW7 (Fig. 2b), which impair the recognition of its substrates (e. g. CCNE1) and subsequent substrate degradation through E3 ligase. In addition, such *FBXW7* mutations were identified in four additional cell lines, EMTOKA (p.R505C), JHUEM3 (p.R465H), VOA8492 (p.R505C) and KLE (p.R479Q) (Fig. 2B). The hotspot mutation of *PPP2R1A* at p.P179, p.R183 or p.S256 sites, which occurs in >20% p53abn EC and mutually exclusive to *FBXW7* mutation, was only detected in HEC50B (p.R183W) (Fig. 2b). No mutations were found in homologous recombination repair genes, *e. g. BRCA1* or *BRCA2*. Although *ARID1A* mutation is rare in p53abn EC, its co-occurrence has been shown to drive the development of aggressive EC in mice[25]. Analysis of p53abn EC cell lines revealed that EFE184, HMMT, JHUEM3, and SPAC1L cells have *ARID1A* deleterious mutations (Fig. 1b). Western blotting analysis verified the complete loss of ARID1A in SPAC1L and EFE-184 cells (Fig. 1c), indicating that these two cell lines represent ARID1A-deficient p53abn EC cell lines. Taken together, these data highlight the genomic similarity between p53abn EC primary tumors and cell lines, the latter serving as a powerful resource for translational research.

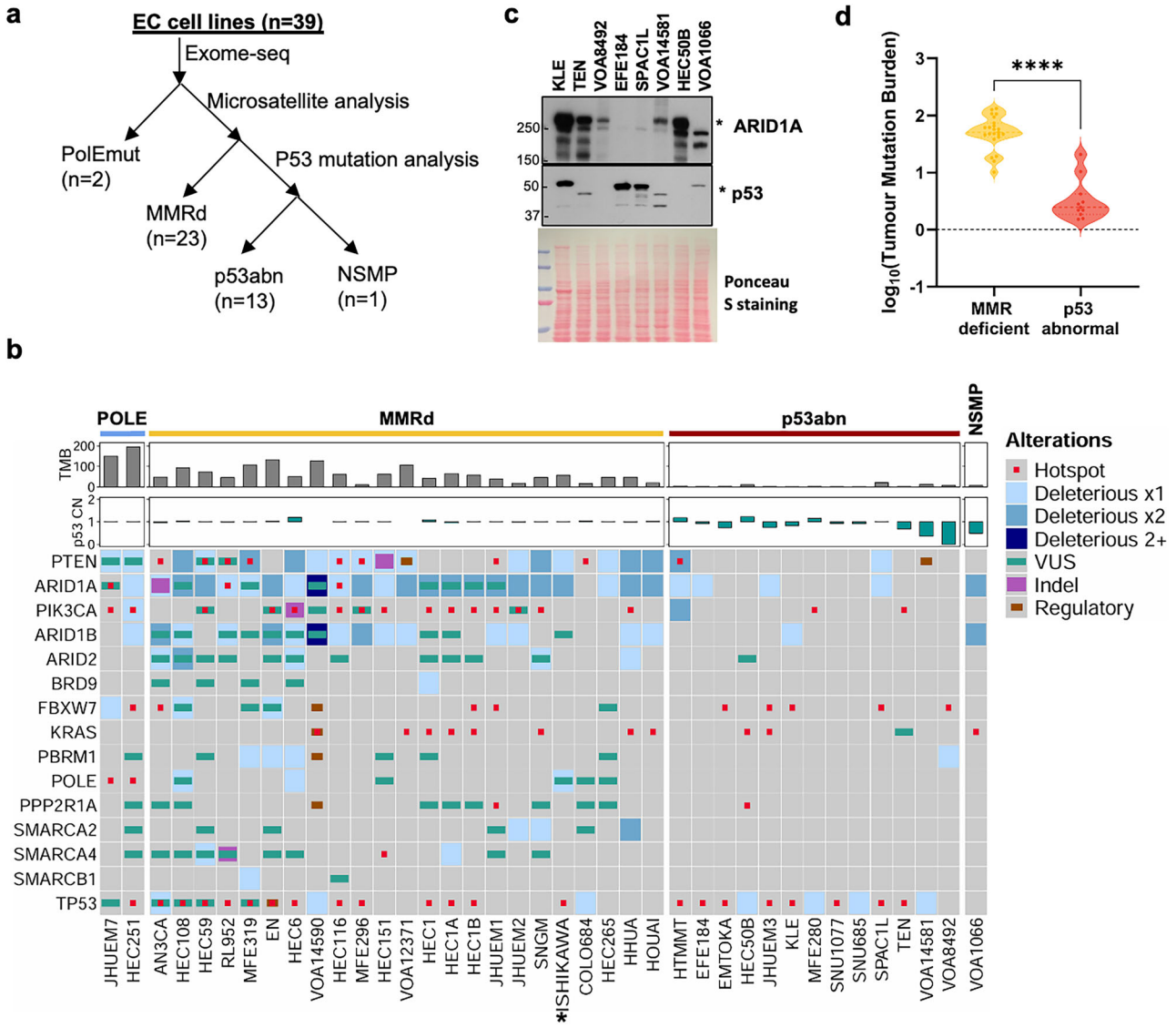

Fig. 1 | Molecular subtyping of endometrial carcinoma cell lines by the ProMisE classifier. a Schematic view of molecular subtyping of EC cell lines. **b** Heatmap of top mutated genes in EC cell lines ordered by their molecular subtypes. *ISHIKAWA refers to (Heraklio)02 ER-, a subclone of ISHIKAWA. **c** Western blotting analysis of p53 and ARID1A expression in p53abn EC cells. **d** Comparison of mutation burden between MMRd and p53abn EC cell lines.

MMRd EC cell lines accumulate frequent p53 and SWI/SNF mutations

The high mutation rate in MMRd EC due to microsatellite instability can lead to the accumulation of additional oncogenic mutations, including *TP53* and SWI/SNF genes, that are prevalent in DD/UDECs (mostly MMRd EC)[26]. In all 23 MMRd cell lines, 14 have at least one hotspot missense or deleterious *TP53* mutation (Fig. 1b), suggesting a selective pressure for accumulating *TP53* mutations during tumor progression or prolonged cell culture. Moreover, multiple cell lines contain mutations of SWI/SNF genes that commonly occur in DD/UDECs. In particular, *ARID1A* and *ARID1B* are mutated in 91% (21/23) and 74% (17/23) of these cell lines, respectively (Fig. 1b). In addition to VOA1066, which was established by us from a UDEC patient with ARID1A/B dual loss[27], AN3CA, EN, MFE-296 and VOA14590H cell lines all harbor two deleterious mutations in each of *ARID1A* and *ARID1B* genes (Fig. 1b), suggestive of their protein loss. Accordingly, MFE-296 was previously confirmed negative for both ARID1A and ARID1B[28]; our western blotting analyses confirmed ARID1A/B dual loss in AN3CA and EN cells, but not those with only one deleterious mutation (Fig. 3a, Supplementary Fig. S3). Similar to VOA1066, PAX8, a lineage marker of differentiated endometrial epithelium, was also absent in AN3CA and EN cells (Fig. 3a, Supplementary Fig. S3), suggesting that they were potentially derived from ARID1A/B-dual deficient DD/UDEC tumors. In addition, VOA14590H was derived from a DDEC primary tumor and formed subcutaneous xenograft tumor with undifferentiated histology and dual loss of ARID1A/B protein (Fig. 3b), indicating that VOA14590H is a bona fide ARID1A/B-dual deficient DDEC cell line. Furthermore, a single *SMARCA4* inactivating mutation was found in two cell lines, HEC1A and HEC59, but no accompanying protein loss was identified in HEC59 cells by western blotting (Fig. 3a, Supplementary Fig. S3). Thus, MMRd EC cell lines exhibited a high tendency to accumulate additional progression events, particularly *TP53* and *ARID1B* mutations, mirroring those in primary tumors.

Tumorigenicity of EC cell lines

Next, we inoculated all available MMRd and p53abn cell lines into immunodeficient mice to determine their capability to induce tumor formation (tumorigenicity). All of the 8 MMRd cell lines available for xenografting, including HEC59, HEC1B, HEC116, VOA12371, AN3CA, EN, HOUA-I, and VOA14590H, developed subcutaneous tumors with various time intervals between cell inoculation and tumor onset (latency) and distinct

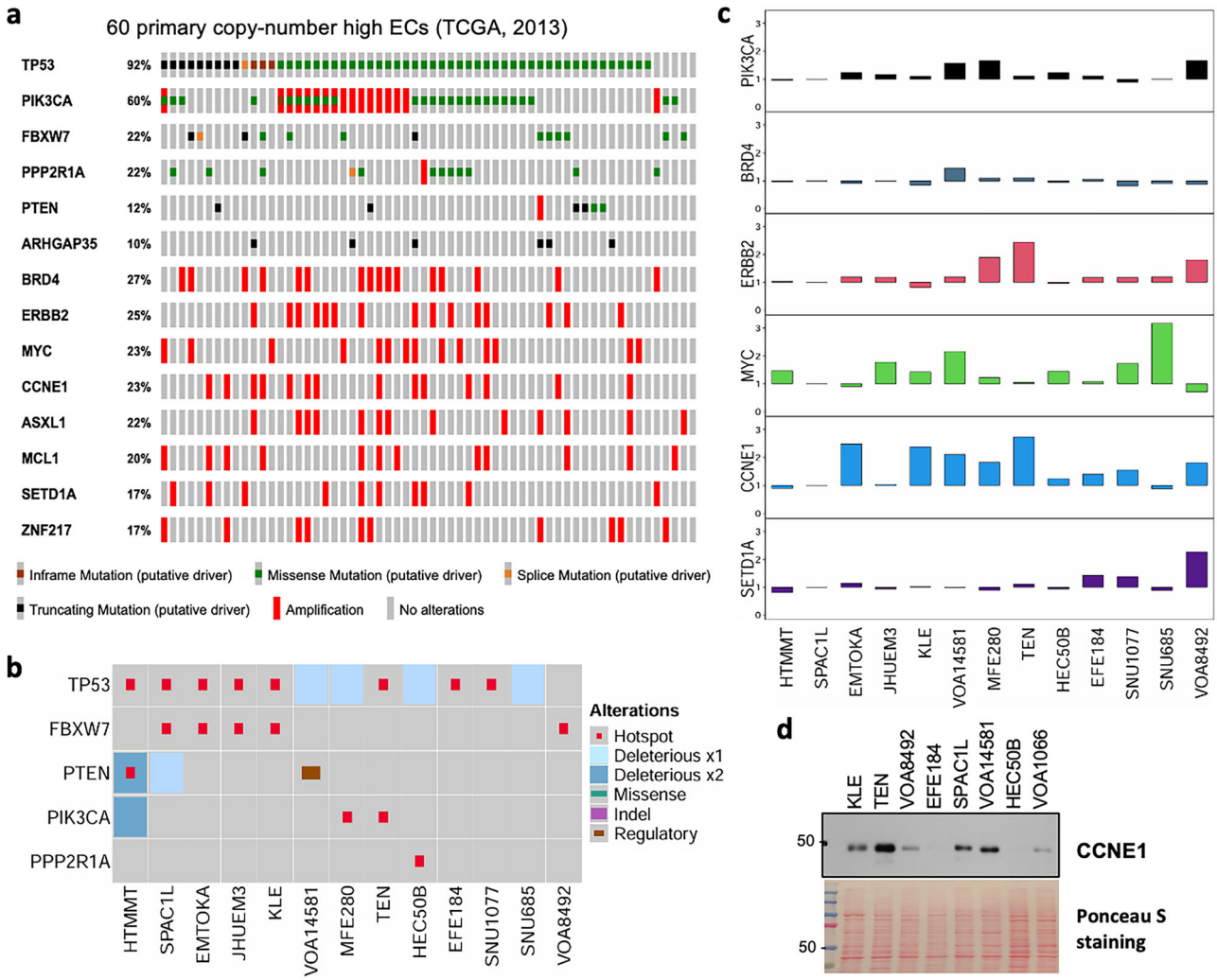

Fig. 2 | Characterization of p53abn EC primary tumors and cell lines. a Heatmap of top mutated/amplified genes in 60 copy number-high ECs (p53abn ECs) sequenced by TCGA; Heatmap of top mutated genes (**b**) and copy number changes of key genes (**c**) in p53abn EC cell lines. SPAC1L, VOA14581, and VOA8492 were sequenced locally and the rest were sequenced by TCGA; **d** Western blotting revealed the protein expression of CCNE1 in EC cell lines.

tumor volume doubling time (Fig. 4a). Histology assessment revealed diverse histology, ranging from intermediate (HEC59, HOUA-I) or poorly differentiated (HEC1B, HEC116, VOA12371) to undifferentiated (AN3CA, EN, VOA14590H) (Figs. 3b and 4b, Supplementary Fig. S4a), further supporting that AN3CA, EN and VOA14590H are representative cell lines of ARID1A/B-dual deficient DD/UDEC. Furthermore, western blotting and IHC staining revealed the expression of dominant-negative mutant p53 in 5 out of 9 tested MMRd cell lines, including HEC59, HEC1B, HEC116, EN and AN3CA (Supplementary Fig. S4b, Fig. 4b), corresponding to the presence of hotspot missense *p53* mutation in these cell lines (Fig. 1b). Among the 7 p53abn EC cell lines tested, including VOA8492, VOA14581, SPAC1L, HEC50B, KLE, EFE-184 and TEN, 4 (HEC50B, SPAC1L, VOA8492 and TEN) developed subcutaneous tumors (Fig. 4a). Histology assessment revealed that SPAC1L and VOA8492 xenografted tumors exhibited papillary serous endometrial carcinoma histology (Fig. 4c), corresponding to the diagnosis of their primary tumors[29] (Supplementary Fig. S5), whereas HEC50B and TEN displayed features of high grade endometrioid carcinoma and clear cell endometrial carcinoma, respectively (Fig. 4c), consistent with the diagnosis of their primary tumors[30,31]. Immunostaining revealed negative p53 staining in VOA8492 and HEC50B cells and domain-negative mutant p53 overexpression staining patterns in SPAC1L and TEN cells (Fig. 4c). SPAC1L was also negative for ARID1A staining (Fig. 4c), supporting it as an *ARID1A*-mutant p53abn EC cell line.

Selective genetic dependencies in p53abn and MMRd EC cells

To provide an example of how molecular classification can advance EC research, we employed the DepMap CRISPR screen database to identify genetic dependencies preferentially in each non-*POLEmut* molecular subtype. DepMap determines genetic dependencies, reported as gene effect scores, by calculating the effect of knocking out individual genes on cell fitness in >1000 cancer cell lines. Analyzing the data available for 25 EC cell lines, including 9 p53abn and 16 MMRd ECs, revealed a great number of lethal genes (gene effect scores: negative values) in each molecular subtype (Supplementary Data 3). When comparing p53abn to MMRd EC cell lines, we identified multiple genes whose deletion was selectively lethal to each molecular subtype (Fig. 5a, Supplementary Data 3). This includes *WRN* for MMRd cells and *CDK2*, *CCNE1*, and *KIF18A* for p53abn cells. WRN was previously shown to be a lethal target in cancer cells with microsatellite instability[32] and inhibition of KIF18A was known to preferentially suppress the growth of p53-mutant ovarian and breast cancer cells[33]. As many of the p53abn EC cell lines have *CCNE1* amplification or *FBXW7* inactivating mutations (Fig. 2b, c), it is also not surprising that these cell lines were more vulnerable to the depletion of either *CCNE1* or *CDK2*, the latter encoding the canonical interacting partner of CCNE1. Therefore, these findings confirm the validity of our analysis approach in identifying molecular subtype-specific lethal targets. Notably, our analysis identified that inactivation of *PELO*, encoding a RNA translation quality control factor[34],

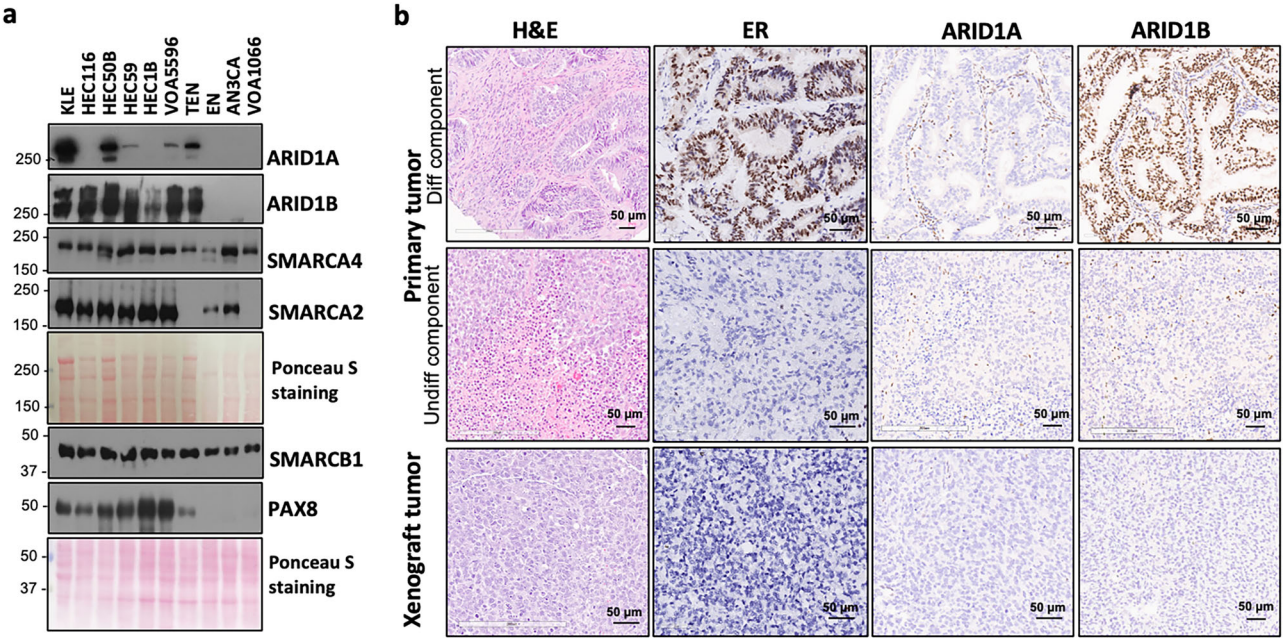

Fig. 3 | Identification of ARID1A/B-dual deficient DD/UDEC cell lines. a Western blotting analysis of SWI/SNF protein and PAX8 expression in EC cell lines. **b** Histology and immunohistochemical features of VOA14590 primary tumor and the cell line-derivative xenograft tumors.

displayed the highest preference in suppressing the growth of MMRd EC cells versus p53abn EC cells (Fig. 5a, Supplementary Data 3). Using CRISPR/Cas9, we demonstrated that *PELO* deletion selectively suppressed the growth of MMRd EC cell lines, HEC1B and HEC116, but not p53abn EC cell lines, HEC50B and TEN (Fig. 5b, c, Supplementary Fig. S6). Therefore, our approach was able to identify novel synthetic lethal targets for specific molecular subtypes of EC.

ARID1A/B-dual deficient DD/UDEC cells rely on mitochondria oxidative phosphorylation

Because DD/UDEC represents one highly lethal histologic subtype of EC that is under-studied, there is an unmet need to identify specific lethal targets in ARID1A/B-dual deficient DD/UDEC. Since the DepMap CRISPR/Cas9 database only included two identified ARID1A/B-dual deficient DD/UDEC cell lines, EN and MFE-296, it does not enable statistical comparison of gene dependency between ARID1A/B-dual deficient cell lines and other EC cell lines. Thus, we searched for *ARID1A* and *ARID1B* deleterious mutations in all CCLE cell lines (Supplementary Data 4), leading to the identification of two more cell lines, EFO-27 and SKUT1, each harboring 2 deleterious *ARID1A* mutations and 2 deleterious *ARID1B* mutations, an indicator of their protein loss supported by our findings in DD/UDEC cells (Figs. 1b and 3b). EFO-27 was derived from endometrioid ovarian cancers, which arise from extra-uterine endometrial epithelial cells and share histopathological and genomic features with endometrioid EC. Immunoblotting confirmed ARID1A/B dual loss in EFO-27 (Supplementary Fig. S7). SKUT1 was derived from uterine tumors with carcinosarcoma features in 1977[35]. Since uterine carcinosarcoma shares common features with DDEC[36] and DD/UDEC has only been recognized in the past 2 decades, it remains possible that the patient tumor, from which SKUT1 cells were derived, was a DDEC or contained a minor undifferentiated component with ARID1A/B dual deficiency. Therefore, these two cell lines were grouped with EN and MFE-296 as ARID1A/B-dual deficient DD/UDEC cell lines for preferential essential gene analysis. In comparison to 27 EC cell lines without ARID1A/B dual loss, these 4 ARID1A/B-dual deficient cell lines are selectively lethal to the loss of genes involved in mitochondria function (Fig. 6a, Supplementary Data 5), which is in line with our previous finding that SMARCA4/2-deficient ovarian and lung tumors rely on mitochondrial oxidative phosphorylation[37].

To assess the potential dependency on mitochondrial oxidative phosphorylation in ARID1A/1B-dual deficient DDEC, we evaluated the efficacy of IACS-010759, a highly selective mitochondrial electron transport chain complex I inhibitor[38], in a panel of EC cell lines. With the Seahorse Cell Mito Stress assay, which uses serial injections of chemical modulators of mitochondria to reveal different aspects of their function, we confirmed thatIACS-010759 inhibited mitochondrial basal and ATP-linked respiration, indicated by the reduced oxygen consumption rate (OCR), in two DD/UDEC cell lines tested (Fig. 6b, Supplementary Fig. S8). Remarkably, IACS-010759 suppressed the growth of ARID1A/1B-dual deficient DDEC cells (Fig. 6c, d), but had little effect on the growth of ARID1A/1B-proficient EC cells (Fig. 6c). In addition, daily treatment of IACS-010759 for 10 days significantly suppressed the tumor growth of VOA1066 cell line-xenografted tumors in immunodeficient mice (Fig. 6e, f) without observable toxicity at necropsy. Lastly, to assess whether dual loss of ARID1A/B creates a dependence on mitochondria function, we inactivated *ARID1B* by CRISPR/Cas9 in HEC1B (Fig. 6g, Supplementary Fig. S9), an ARID1A-deficient/ARID1B-proficient EC cell line, which significantly increased the cellular sensitivity to IACS-010759 treatment (Fig. 6h). Taken together, these data indicate that ARID1A/1B-dual deficiency conferred increased cellular sensitivity to the inhibition of mitochondria electron transport chain activity.

Discussion

Cancer cell lines are crucial tools in cancer research as they provide consistent and reproducible models for studying disease biology and developing therapeutics. However, the reliability of cancer cell lines in modeling disease depends on the original diagnosis when the cell lines were established, and may be questioned as our understanding of the disease evolves. Therefore, the proper classification of cell lines is critical for their application in basic and translational cancer research. We have previously reclassified multiple gynecologic cancer cell lines based on genomic understanding of the relevant diseases and histologic reassessment[16], leading to an improved representation of molecularly defined ovarian cancer cell lines in large-scale functional genomic screen studies and subsequent identification of targetable genetic dependencies in those molecularly defined ovarian cancer subtypes[37]. In this study, we classified EC cell lines into the more recently recognized clinically relevant ProMisE molecular subtypes and the

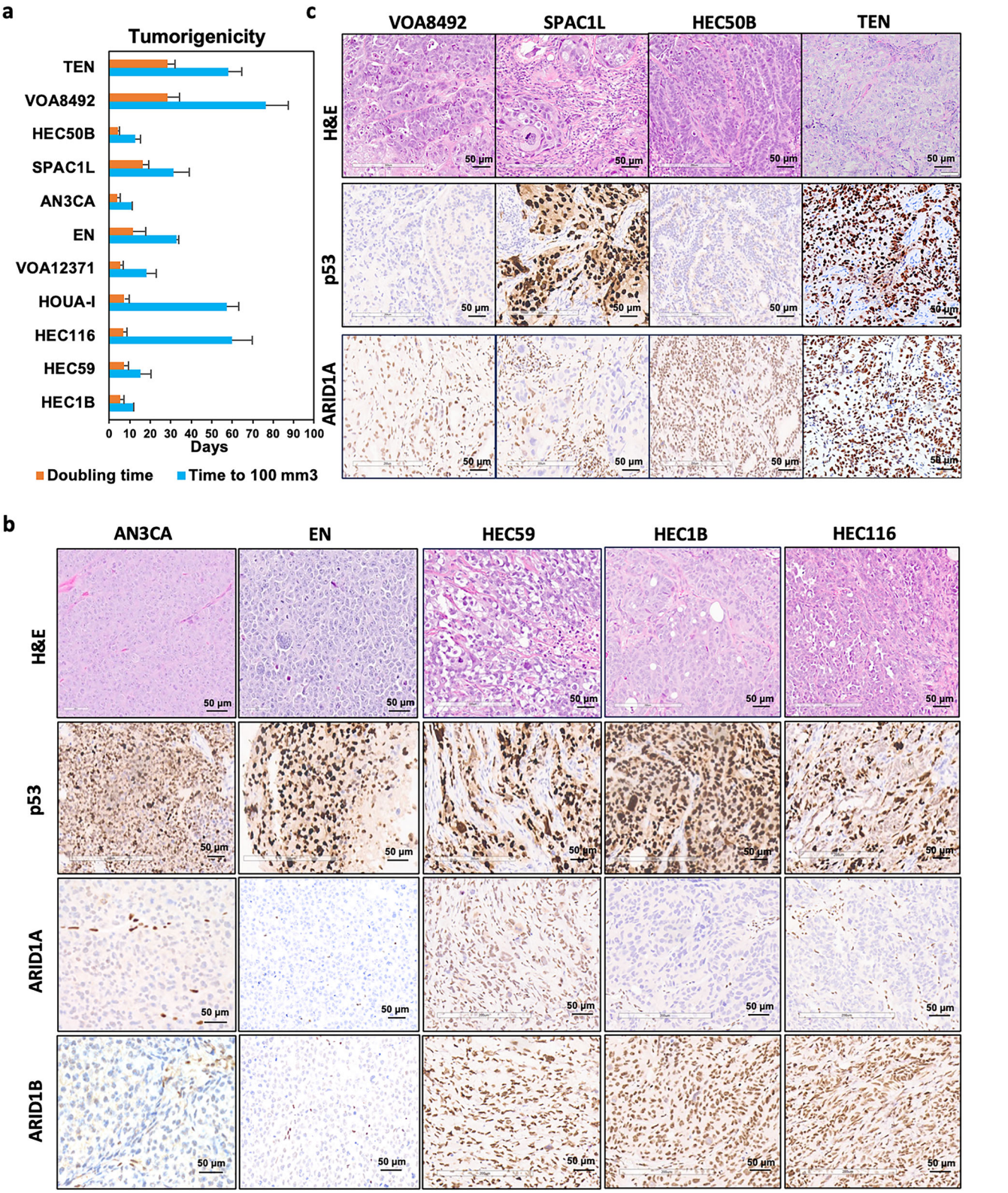

Fig. 4 | Tumorigenicity of MMRd and p53abn EC cell lines. a Xenografted tumor development of indicated EC cell lines in immunodeficient female NRG mice ($n = 4$). Tumorigenicity, capability to induce tumor formation; latency, time intervals (days) between cell inoculation and measurable tumor size (~100 mm^3)"; doubling time, days for tumor volume increasing from ~200 to 400 mm^3. Error bars represent SD. **b** Histology and immunohistochemical features of xenograft tumors of MMRd EC cell lines. **c** Histology and immunohistochemical features of xenograft tumors of p53abn EC cell lines.

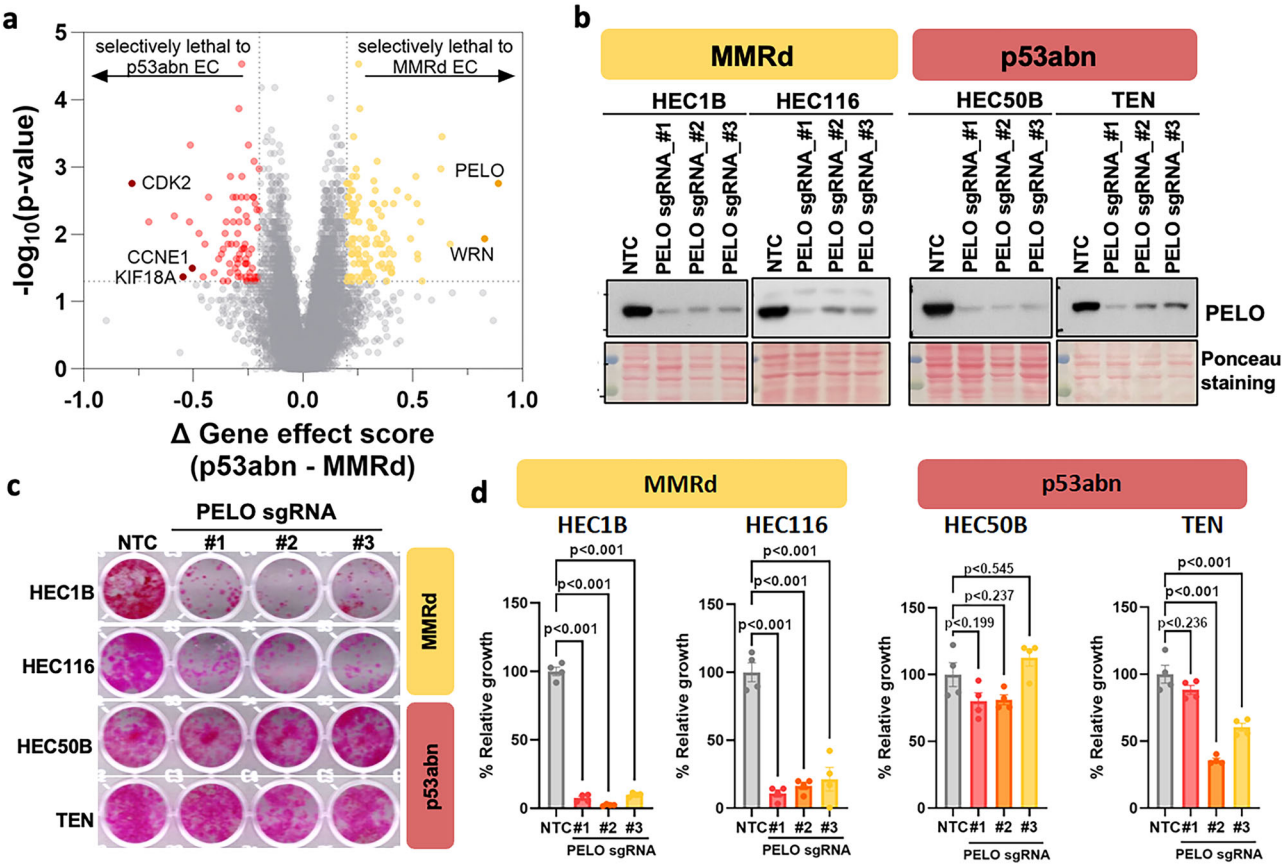

Fig. 5 | Identification of selective genetic dependencies in p53abn and MMRd ECs. a Comparison of genetic dependency in 16 MMRd EC cell lines vs 9 p53abn EC cell lines. Genome-wide CRISPR screen data was downloaded from the DepMap database (23Q2). MMRd EC cell lines: COLO684, MFE296, JHUEM1, HEC1B, HEC265, ISHIKAWAHERAKLIO02ER, RL952, SNGM, EN, HEC6, MFE319, HEC59, HEC1, HEC116, HHUA and HOUAI; p53abn EC cell lines: MFE280, KLE, SNU1077, TEN, SNU685, EFE184, HEC50B, EMTOKA and HTMMT. **b** Western blotting showing PELO knockout by CRISPR/Cas9 in MMRd and p53abn EC cells. Representative images (**c**) and quantitation (**d**) of the effect of PELO deletion on the growth of MMRd EC cell lines. Error bars represent SEM and p-values were determined using Tukey multiple comparison test.

ARID1A/B-dual deficient DD/UDEC molecular subtype, which will guide the future use of these cell lines for identifying and/or validating novel therapeutics for each molecular subtype. Notably, only one NSMP cell line (2.6%) was identified, which is significantly lower than the 50% representation observed for NSMP subtype in primary ECs[5,6]. This discrepancy could be due to the low-grade nature of most NSMP ECs and the lack of genomic instability that does not allow for the rapid selection of subclones with increased fitness during prolonged culture. Supporting this, VOA1066, the only NSMP cell line identified, is indeed an ARID1A/B-dual deficient UDEC cell line[27]. Future work is needed to develop additional cell lines from high-grade NSMP ECs to facilitate the research.

Capitalizing on the molecular classification of EC cell lines by the ProMisE classifier, we identified putative targetable features specific to MMRd and p53abn ECs, respectively, through analyzing a publicly available database, created by DepMap, of the genome-wide CRISPR knockout screens on EC cell lines. For MMRd EC cell lines, our discovery of their sensitivity to *PELO* deletion agrees with a recent report describing PELO dependency in microsatellite instable cells by Borck et al.[39] during the preparation of this manuscript. As a component of the Pelota-HBS1L complex, PELO recognizes ribosomes stalled at the 3'end mRNAs to promote its disassembly and subsequent degradation of damaged mRNAs[34,40,41]. Borck et al. further demonstrated that *TTC37*, a gene encoding an integral component of the superkiller complex that extracts RNA from stalled ribosomes, is frequently repressed due to microsatellite mutations in MMRd cells and *PELO* deletion further destroyed the RNA quality control, leading to the accumulation of misfolded/unfolded nascent polypeptides and subsequent cell death[39]. Future development of PELO inhibitors will allow for the assessment of their therapeutic potential in MMRd ECs, particularly those not responsive to immune therapy.

For p53abn ECs, our finding of their dependencies on CDK2 and KIF18A is supported by other studies. CDK2 is a cyclin-dependent kinase that pairs with E- and A-type cyclins during S and G2 cell cycle phases. It has multiple roles in cell cycle checkpoint control and its function is often redundant with that of CDK1[42,43]. However, in the absence of p53, CDK2 is essential for G2/M checkpoint control and is non-redundant with CDK1[44]. Moreover, p53 can repress CDK2 during DNA damage or oncogene-induced cellular senescence, and inhibition of CDK2 can decrease the tumor penetrance and delay tumor onset in p53-null pineal tumor cells[45]. Notably, it is also reported that CDK2 is critical for repairing the collapsed replication fork in *CCNE1*-amplified ovarian cancer cells[46]. As several of these p53abn EC cell lines have amplified *CCNE1* and/or stabilized CCNE1 protein due to FBXW7 inactivation, the dependence on CDK2 in p53abn EC cell lines could be attributed to both p53 abnormality and CCNE1 hyperactivation. Furthermore, KIF18A motor protein utilizes ATP hydrolysis to move along kinetochore-microtubule fibers[47]. It has been discovered that KIF18A is a selective genetic dependency in chromosome-unstable cancer cell lines, such as p53-mutant cancer cells[33,48–50]. Notably, selective inhibitors of KIF18A and CDK2 are being tested in clinical trials of various cancers (NCT06799065, NCT05902988, NCT05262400, NCT05252416). In particular, ATX-295, a KIF18A inhibitor, has been recently granted a fast-track

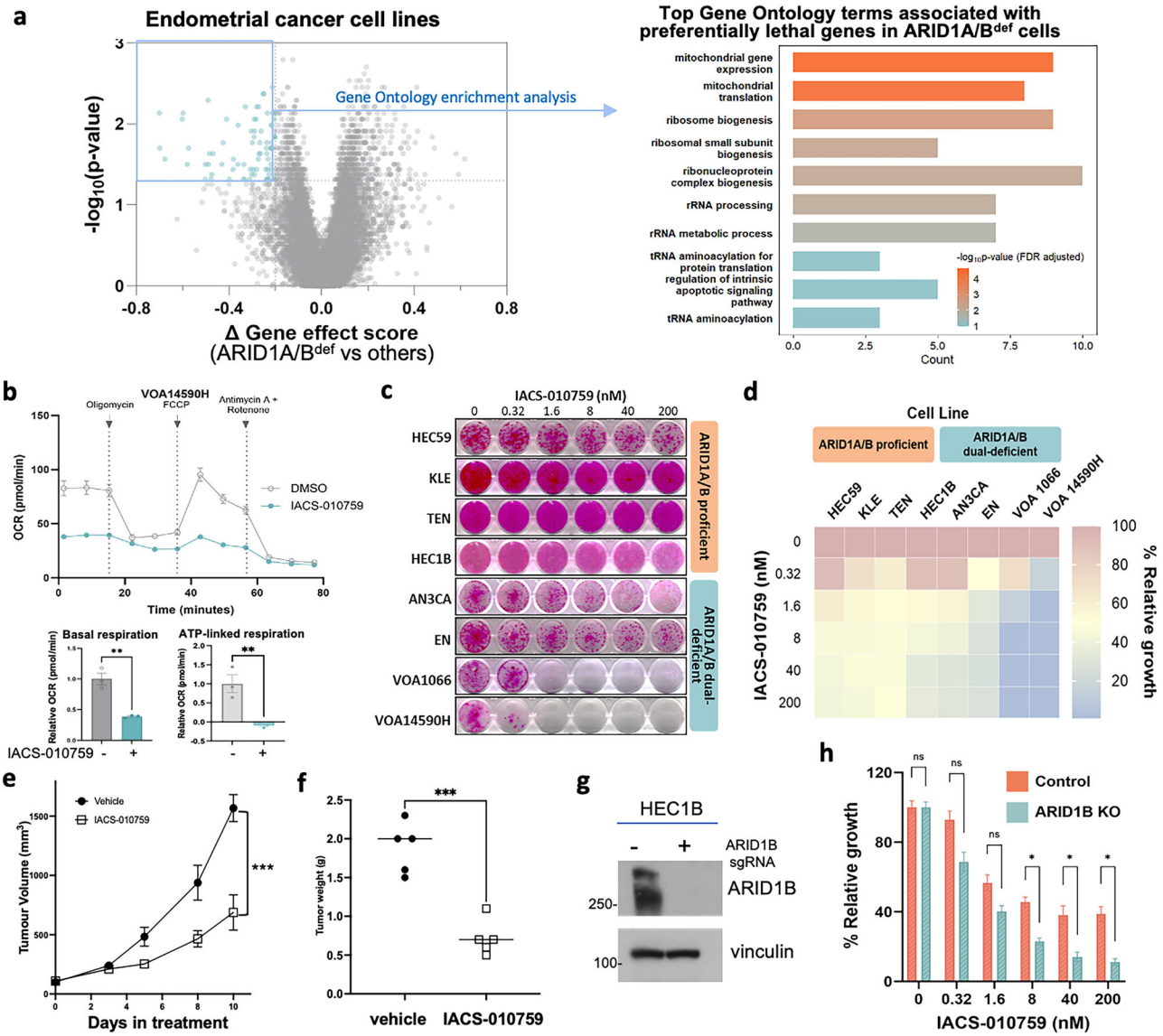

Fig. 6 | ARID1A/B-dual deficient DD/UDEC cells depend on oxidative phosphorylation. a Left, a volcano plot showing the differential genetic dependency of genes between *ARID1A/B*-deficient ($n = 4$: EN, MFE-296, EFO-27, and SKUT-1) and proficient ($n = 27$) EC cell lines, which includes 2 *POLEmut* (HEC251 and JHUEM7), 16 MMRd, and 9 p53abn (detailed in Fig. 5 legend). The genetic dependency was calculated using the CERES gene effect data from DepMap genome-wide CRISPR/Cas9 screens. Significance was assessed using Wilcoxon rank-sum test. Each dot denotes a gene. Genes highlighted in blue represent those whose deletion selectively impairs the growth of *ARID1A/1B*-deficient cell lines and were subjected to Gene Ontology enrichment analysis. Right, bar graph reflecting the GO analysis of the highlighted genes essential for *ARID1A/1B*-deficient cancer cells. **b** OCR was measured with the Seahorse Mito Stress test for VOA14590H cells treated with and without IACS-010759 (2 nM for 1 h). Bar graphs show relative basal respiration. **c** Representative images of a panel of endometrial cancer cell lines treated with varying concentrations of IACS-010759 for 12–22 days. **d** Relative growth of ARID1A/B-proficient and dual-deficient cells treated with IACS-010759 for 12–22 days. Effects of IACS-010759 treatment on the growth of VOA1066 cell line-derived xenografted tumors, measured by tumor volume (**e**) and final tumor weights (**f**). **g** Western blotting showing *ARID1B*-knockout in HEC1B cells. **h** Bar graph showing relative growth of HEC1B cells, ±*ARID1B*-knockout, treated with IACS-10759 for 10–12 days. Error bars represent SEM and p-values were determined using unpaired t-test, corrected for multiple comparisons using the Bonferroni–Dunn method. $^{*}p < 0.05$, $^{**}p < 0.01$, $^{***}p < 0.001$.

designation by the U.S. Food and Drug Administration for the treatment of adult patients with advanced/metastatic platinum-resistant or refractory ovarian cancer, suggesting a rapid pathway for knowledge translation.

ARID1A/B-dual deficient DD/UDEC has been recently recognized as a highly lethal EC subtype. In addition to the first UDEC cell line, VOA1066, from a primary tumor with ARID1A/B dual deficiency[27], this cell line has a low mutation burden, normal p53 expression, and is classified as an NSMP cell line, supporting the notion that DD/UDEC can arise from NSMP ECs, and represents a highly lethal outlier of NSMP ECs that are otherwise innocent. Our present study further established the VOA14590H cell line from an ARID1A/B-dual deficient primary DDEC tumor and identified three more ARID1A/B-dual deficient EC cell lines, EN, AN3CA, and MFE-296. All four of these cell lines are MMRd and representative models ofARID1A/B-dual deficient DD/UDECs with MMRd. Notably, VOA14590H was developed independently from the same primary tumor that was utilized for developing the DDEC-3 cell line by Wong et al.[51]. Future genomic analysis is required to determine whether these two cell lines can be considered as the same cell line. Furthermore, our study also identified that SKUT1 may arise from a primary tumor representing or containing a component of DD/UDEC with ARID1A/B dual deficiency, rather than the original diagnosis of carcinosarcoma. This finding is critical as it will allow for the proper use of this cell line for future basic and translational studies.

Moreover, our study also demonstrated that EFO-27, which originated from an ovarian endometrioid carcinoma, represents an ARID1A/B-dual deficient DD/UDOC cell line. However, as none of the primary tumors used to establish EN, AN3CA, MFE-296, SKUT1, and EFO-27 are available for reinvestigation, it remains possible that dual-loss of ARID1A and ARID1B may accumulate during prolonged culture, as all of these cell lines are hypermutated, which can facilitate the emergence and selection for these aggressive clones. Nevertheless, we also demonstrated that ARID1A/B dual deficiency in EC, mimicking SMARCA4/2-dual deficiency[37], creates a dependency on oxidative phosphorylation, indicating that patients with these highly lethal SWI/SNF-mutant cancers can be included in a basket clinical trial to test the efficacy of mitochondria-targeting therapeutic approaches. Notably, although IACS-010759, an electron transport chain complex I inhibitor[38], displayed a narrow therapeutic index in clinics[52], its hyperactivity in these SWI/SNF-mutant cancer cells suggests that IACS-010759 may be effective at tolerable doses in these cancers, which requires future clinical investigation.

Lastly, our study also assessed the tumorigenicity of MMRd and p53abn EC cell lines in immunodeficient mice. As these EC cells largely recapitulate the genomic features of patient tumors, their derivative xenografts can complement EC patient-derived xenografts[53], which resemble patient tumors more closely but are often challenging to share freely across institutions, to facilitate future translational research. Among the four p53abn EC cell line xenografts, TEN and VOA8492 developed tumors with long latency and long doubling time (Fig. 4a), which limits their utility for translational research. In contrast, HEC50B and SPAC1L developed tumors rapidly and are thereby suitable for preclinical testing of therapeutic candidates (Fig. 4a). Several p53abn cell lines, including KLE, VOA14581, and EFE-184, failed to develop subcutaneous tumors in our study, limiting their usage for in vivo validation of putative novel therapeutics. Noticeably, Gao et al. isolated CD44 and CD133-positive tumor-initiating cells from KLE, which were able to develop subcutaneous tumors in athymic nude mice[54]. KLE was also able to develop slow-growing orthotopic tumors[55] or lung metastasis through tail vein injection[56] in nude mice. Therefore, additional model development studies are necessary to further determine the growth behaviors of TEN and VOA8492 and also to validate the tumorigenicity of VOA14581 and EFE-184 in immunocompromised mice to determine their potential in translational research. Given their heterogeneity and aggressiveness, more p53abn EC cell lines are needed for translational research.

Taken together, our study provides the molecular classification of EC cell lines to accelerate basic and translational research in EC. In particular, ARID1A/B-dual deficient DD/UDEC cells are selectively sensitive to pharmacologic inhibition of mitochondrial oxidative phosphorylation in vitro and in vivo, which warrants clinical investigation to inform the design of an optimal treatment approach for these highly aggressive cancers.

Methods

Cell lines and patient tissues

HEC50B, TEN, HOUA-I, HEC59, HEC116, HEC1B, KLE, EFE-184, SPAC-1L, AN3CA, EN, and EFO-27 cells were grown in RPMI media supplemented with 5% characterized FBS (Corning, cat # CA76322-116) and grown at 37 °C in a 5% CO_2 incubator.

To establish cell lines from patients' specimens, primary tumor tissues or ascites were collected under the University of British Columbia Ethics Board protocol H02-61375 and H18-01457, at the time of surgery after obtaining an informed consent from the patients. For VOA8492, VOA14581, and VOA14590H cell lines, tumor tissues were minced and digested in 2.5 mg/mL Collagenase D (Sigma-Aldrich, cat#11088882001). After 60 min, single cells from the solution were placed into Petri dishes with 199:105 media, consisting of a 1:1 ratio of media 199 (Thermofisher Scientific, cat# 31100035) and media 105 (Sigma-Aldrich, cat# M6395) fortified with 10% defined FBS (Hyclone, cat# SH30070.03) and 10 µg/mL of Gentamicin (Thermofisher Scientific, cat# 15710064). For the VOA12371 cell line, cells from ascites were lysed with ammonium chloride to remove red blood cells. Primary cells were left to adhere and grow at 37 °C in a 5% CO_2 incubator with culture medium replaced every 3–4 days. Cancer cells were enriched by differential trypsinization and subsequent removal of fibroblasts, and continuously passaged for at least 20 passages to ensure the establishment of cell lines.

All cell lines were certified by the short tandem repeat (STR) analysis through LabCorp, tested regularly for *Mycoplasma* (Genetica, DNA Laboratories), and used for the study within 6 months of thawing from liquid nitrogen storage. The STR profiles of four newly developed EC cell lines were reported in Supplementary Table S2.

Exome sequencing, mapping and variant calling

The whole exome sequencing datasets available for EC cell lines were downloaded from the DepMap database (www.depmap.org; 2023Q2). Whole-exome data of VOA1066 cell line was obtained from our previous study[27]. We also performed whole-exome sequencing on SPAC1L and two in-house developed EC cell lines, VOA8492 and VOA14581, as well as their respective normal DNA from buffy coat samples. Briefly, genomic DNA isolated from cells and patients' buffy coats were fragmented to a target size of 150–200 bp on the Covaris E210 system and the whole-exome was sequenced as previously described in ref. 13. Fastq files were aligned with Burrows-Wheeler Aligner (BWA) 0.7.5a to hs37d5, and the SAM output file was converted into a sorted BAM file using SAMtools 0.1.19. BAM files underwent indel realignment, duplicate marking and recalibration steps in this order with the Genome Analysis Toolkit (GATK) 2.8-1, where dpsnp137 was used for known SNPs and Mills_and_1000G_gold_ standard.indels.b37.vcf was used for known indels. Variant calling was carried out in tumor-only mode with HaplotypeCaller, and output VCF files were recalibrated with VariantRecalibrator from GATK 2.8-1. SnpEff 3.2 and SnpSift 1.9c were then used to annotate these VCF files with database version GRCh37.70. Only variants with a minimum quality score of 20 were extracted. Thereafter, we excluded variants with a Global Minor Allele Frequency >= 0.01 and those somatic nucleotide variants (SNVs) that either appeared in the 1000 Genomes Project database, the dbSNP database or the National Heart, Lung, and Blood Institute (NHLBI) Exome Sequencing Project database, assuming that these SNVs might be of less importance for tumorigenesis. Somatic copy number analysis was completed following the GATK tutorial "(How to part I) Sensitively detect copy ratio alterations and allelic segments" and verified using Novogene copy number analysis (copy number called using Control-FREEC).

Targeted panel sequencing

We performed targeted cancer gene panel sequencing for VOA12371 cell line and VOA14590H xenograft tumor using the QIAseq Comprehensive Cancer Panel as previously described[24]. The resulting raw Fastq files were uploaded to QIAseq's cloud-based processing portal GeneGlobe. Using this portal, we ran the QIAseq-developed processing pipeline for trimming, alignment, post-processing, and mutation calling against the reference genome hg19. Subsequently, results for all samples were concatenated, and extensive mutation filtering was performed manually to remove artifacts. Output files for all samples were combined so that common germline SNPs and artifacts could be removed. Further filtering using gnomAD and ClinVar[57,58] was performed to filter out more germline SNPs and variants with a Global Minor Allele Frequency ≥0.01. Additionally, all "modifier" mutations occurring far from splice sites were removed.

Genome-wide CRISPR screen data analysis

CRISPR/Cas9 knockout data was downloaded from the DepMap database (www.depmap.org; 2023Q2). Differential gene dependency was determined by using a two-sided Wilcoxon rank sum test to compare the DepMap CRISPR knockout data gene effect scores between MMRd and p53abn EC cell lines or between ARID1A/B dual-deficient cell lines and the remaining EC cell lines with available screen data.

Western blotting

Whole cell lysates were extracted using urea lysis buffer (9 M urea, 4% CHAPS, 0.5% IPG buffer, 50 mM DTT, Sigma-Aldrich). Twenty

micrograms of cell lysate was resolved on SDS-PAGE gels for protein detection. Antibodies against SMARCA4 (Abcam, cat# ab11064, 1:5000), SMARCA2 (Cell Signaling Technology, cat# D9E8B, 1:1000), ARID1A (Sigma-Aldrich, cat# HPA005456, 1:1000), p53 (ProteinTech, cat# 10442-1-AP, 1:3000), SMARCB1 (BDBioscience, cat# 612110, 1:1000), PAX8 (ProteinTech, cat# 10336-1-AP, 1:2000), PELO (ProteinTech, cat#10582-1-AP, 1:2000), CCNE1 (Abcam, cat# ab9517, 1:500). Ponceau S staining and/or Vinculin (Sigma-Aldrich, cat#V9131, 1:10000) were used to confirm equal protein loading.

Immunohistochemistry

Formalin-fixed, paraffin-embedded tissue blocks were sectioned at 4μm thickness onto Superfrost+ glass slides and immunohistochemically stained using the Leica BOND RX system. Antibodies used for immunohistochemistry were previously described in refs. 16,26. Staining was evaluated by one or both gynecologic pathologists (L.H., S.M.).

Gene knockout by CRISPR/Cas9 technology

Knockout of ARID1B and PELO were achieved by a pool of 3 GFP-tagged CRISPR/Cas9 KO plasmids targeting ARID1B (Santa Cruz, sc-402365) or 3 individual CRISPR/Cas9 KO plasmids targeting PELO with the following sgRNA sequences: GGCTTGAGAGTCGAAGTCGA, TGGTCCCCTTA ACCCGCAGC and AGTCCATAGAAAGCTCGATC. These sgRNA sequences were cloned into LentiCRISPR-v2-puro vector (a gift from Feng Zhang, Addgene #52961)[59]. Viral packaging and infection were completed as previously described in ref. 16. GFP-positive or puromycin-resistant pooled cells were harvested for western blotting to confirm target depletion.

Cell growth assays

For measuring cell growth, cells were seeded at 1500 cells/well in quadruplicate in 24-well plates. Plates were fixed when control conditions grew up to 80–100% confluence, which usually takes 8–21 days after plating. To determine cell growth after drug treatment, cells were treated with either vehicle or testing agents 24 h after plating. Treatments were refreshed every 4 days until the control conditions reached confluence. Cells were fixed with 10% trichloroacetic acid (Sigma-Aldrich cat# T6399-500G) before washing. Once plates were dry, the cells were stained with 0.4% (wt/vol) sulforhodamine B (Sigma-Aldrich cat# 230162) dissolved in 1% acetic acid. The stain was dissolved with 10 mM Tris-base pH 10.5 to quantify cell growth that was normalized to relevant control conditions.

Seahorse assays

Mitochondrial OCR were determined using the XF96 Pro Analyzer (Seahorse Bioscience) as previously described in ref. 37. Briefly, cells were seeded at 18,000–40,000 cells/well at 90% confluency in Seahorse XF96 Pro cell culture microplates (Agilent) the day before the experiment. An hour prior to running the assay, cells were refreshed with RPMI supplemented with 2 mM L-glutamine, 10 mM glucose, 1 mM sodium pyruvate and either DMSO or 2 nM of IACS-10759 (ChemieTek, cat# CT-IACS107) adjusted to pH 7.4 and kept in at 37 °C in CO_2-free incubator. Afterwards, plates were loaded on the Seahorse Analyzer followed by sequential injections of oligomycin (Sigma-Aldrich, cat# O4876, FCCP (Sigma-Aldrich, cat# C2920), and a mixture of antimycin A (Sigma-Aldrich, cat# A8674) and rotenone (Sigma-Aldrich, cat# R8875) to a final concentration of 1 μM of oligomycin, 1.5 μM of FCCP, and 1 μM antimycin A, and 100 nM rotenone respectively, at 35, 56, and 77 min. OCR were normalized to the DMSO condition.

Mouse xenograft studies

All procedures related to animal handling, care, and treatment in this study were approved by the Animal Care Committee of the University of British Columbia (A22-0005). Briefly, 5–10 × 10^6 cells per mouse, with a 1:1 mix of Matrigel (Corning) in a final volume of 200 μl, were injected subcutaneously into the back of NRG (NOD.Rag1KO.IL2RγcKO) mice. Tumor volumes and mouse weights were measured twice weekly. Tumor volume was calculated with the following formula: length × $(\text{width})^2 \times 0.52$. Mice were monitored for health until they reached humane endpoints for tumor isolation. Isolated tumors were fixed in 10% neutral buffered formalin and embedded for histology analysis.

Statistical analysis

Unless otherwise specified, the student's *t* test was used to evaluate the significant difference between 2 groups of data in all in vitro experiments. $P < 0.05$ was considered significant.

Data availability

This study used processed sequence data publicly available in the DepMap database (www.depmap.org). The datasets generated for in-house developed cell lines during the current study are not publicly available due to the restriction of research ethics approval but are available from the corresponding author on reasonable request through a material transfer agreement.

Received: 26 April 2025; Accepted: 11 July 2025;
Published online: 24 July 2025

References

1. Setiawan, V. W. et al. Type I and II endometrial cancers: have they different risk factors? *J. Clin. Oncol.* **31**, 2607–2618 (2013).
2. Cancer et al. Integrated genomic characterization of endometrial carcinoma. *Nature* **497**, 67–73 (2013).
3. McConechy, M. K. et al. Use of mutation profiles to refine the classification of endometrial carcinomas. *J. Pathol.* **228**, 20–30 (2012).
4. Kunitomi, H. et al. New use of microsatellite instability analysis in endometrial cancer. *Oncol. Lett.* **14**, 3297–3301 (2017).
5. Kommoss, S. et al. Final validation of the ProMisE molecular classifier for endometrial carcinoma in a large population-based case series. *Ann. Oncol.* **29**, 1180–1188 (2018).
6. Talhouk, A. et al. Confirmation of ProMisE: A simple, genomics-based clinical classifier for endometrial cancer. *Cancer* **123**, 802–813 (2017).
7. Concin, N. et al. ESGO/ESTRO/ESP guidelines for the management of patients with endometrial carcinoma. *Int. J. Gynecol. Cancer* **31**, 12–39 (2021).
8. Leon-Castillo, A. et al. Clinicopathological and molecular characterisation of 'multiple-classifier' endometrial carcinomas. *J. Pathol*. https://doi.org/10.1002/path.5373 (2019).
9. Jamieson, A., Thompson, E. F., Huvila, J., Gilks, C. B. & McAlpine, J. N. p53abn Endometrial Cancer: understanding the most aggressive endometrial cancers in the era of molecular classification. *Int. J. Gynecol. Cancer* **31**, 907–913 (2021).
10. Eskander, R. N. et al. Pembrolizumab plus chemotherapy in advanced or recurrent endometrial cancer: overall survival and exploratory analyses of the NRG GY018 phase 3 randomized trial. *Nat. Med.* **31**, 1539–1546 (2025).
11. Yonemori, K. et al. Analysis of East Asia subgroup in Study 309/KEYNOTE-775: lenvatinib plus pembrolizumab versus treatment of physician's choice chemotherapy in patients with previously treated advanced or recurrent endometrial cancer. *J. Gynecol. Oncol.* **35**, e40 (2024).
12. Silva, E. G., Deavers, M. T., Bodurka, D. C. & Malpica, A. Association of low-grade endometrioid carcinoma of the uterus and ovary with undifferentiated carcinoma: a new type of dedifferentiated carcinoma? *Int. J. Gynecol. Pathol.* **25**, 52–58 (2006).
13. Kuhn, E., Ayhan, A., Bahadirli-Talbott, A., Zhao, C. & Shih Ie, M. Molecular characterization of undifferentiated carcinoma associated with endometrioid carcinoma. *Am. J. Surg. Pathol.* **38**, 660–665 (2014).
14. Tafe, L. J., Garg, K., Chew, I., Tornos, C. & Soslow, R. A. Endometrial and ovarian carcinomas with undifferentiated components: clinically aggressive and frequently underrecognized neoplasms. *Mod. Pathol.* **23**, 781–789 (2010).

15. Busca, A. et al. Undifferentiated endometrial carcinoma arising in the background of high-grade endometrial carcinoma - Expanding the definition of dedifferentiated endometrial carcinoma. *Histopathology* **77**, 769–780 (2020).
16. Karnezis, A. N. et al. Re-assigning the histologic identities of COV434 and TOV-112D ovarian cancer cell lines. *Gynecol. Oncol*., https://doi.org/10.1016/j.ygyno.2020.12.004 (2020).
17. Silva, E. G., Deavers, M. T. & Malpica, A. Undifferentiated carcinoma of the endometrium: a review. *Pathology* **39**, 134–138 (2007).
18. Stewart, C. J. & Crook, M. L. SWI/SNF complex deficiency and mismatch repair protein expression in undifferentiated and dedifferentiated endometrial carcinoma. *Pathology* **47**, 439–445 (2015).
19. Coatham, M. et al. Concurrent ARID1A and ARID1B inactivation in endometrial and ovarian dedifferentiated carcinomas. *Mod. Pathol.* **29**, 1586–1593 (2016).
20. Kobel, M. et al. Undifferentiated endometrial carcinomas show frequent loss of core switch/sucrose nonfermentable complex proteins. *Am. J. Surg. Pathol.* **42**, 76–83 (2018).
21. Strehl, J. D. et al. Pattern of SMARCB1 (INI1) and SMARCA4 (BRG1) in poorly differentiated endometrioid adenocarcinoma of the uterus: analysis of a series with emphasis on a novel SMARCA4-deficient dedifferentiated rhabdoid variant. *Ann. Diagn. Pathol.* **19**, 198–202 (2015).
22. Tessier-Cloutier, B. et al. SWI/SNF-deficiency defines highly aggressive undifferentiated endometrial carcinoma. *J. Pathol. Clin. Res.* **7**, 144–153 (2021).
23. Santoro, A. et al. Clinico-pathological significance of TCGA classification and SWI/SNF proteins expression in undifferentiated/dedifferentiated endometrial carcinoma: a possible prognostic risk stratification. *Gynecol. Oncol.* **161**, 629–635 (2021).
24. Jamieson, A. et al. Targeted and shallow whole-genome sequencing identifies therapeutic opportunities in p53abn endometrial cancers. *Clin. Cancer Res.* **30**, 2461–2474 (2024).
25. Reske, J. J. et al. Co-existing TP53 and ARID1A mutations promote aggressive endometrial tumorigenesis. *PLoS Genet.* **17**, e1009986 (2021).
26. Shin, C. Y. et al. Prognostic values of molecular subtypes and SWI/SNF protein expression in de-differentiated/undifferentiated endometrial carcinoma. *Histopathology*, https://doi.org/10.1111/his.15411 (2025).
27. Wang, Y. et al. Establishment and characterization of VOA1066 cells: An undifferentiated endometrial carcinoma cell line. *PLoS ONE* **15**, e0240412 (2020).
28. Wang, Z. et al. Dual ARID1A/ARID1B loss leads to rapid carcinogenesis and disruptive redistribution of BAF complexes. *Nat. Cancer* **1**, 909–922 (2020).
29. Hirai, Y., Kawaguchi, T., Hasumi, K., Kitagawa, T. & Noda, T. Establishment and characterization of human cell lines from a serous papillary adenocarcinoma of the endometrium. *Gynecol. Oncol.* **54**, 184–195 (1994).
30. Kuramoto, H. et al. Establishment and characterization of human endometrial cancer cell lines. *Ann. N. Y. Acad. Sci.* **622**, 402–421 (1991).
31. Fushiki, H. et al. Characterization of a newly established human tumor cell line (TEN) from a patient with clear cell carcinoma of the uterine body and its sensitivity to anti-cancer agents. *Hum. Cell* **10**, 199–208 (1997).
32. Chan, E. M. et al. WRN helicase is a synthetic lethal target in microsatellite unstable cancers. *Nature* **568**, 551–556 (2019).
33. Payton, M. et al. Small-molecule inhibition of kinesin KIF18A reveals a mitotic vulnerability enriched in chromosomally unstable cancers. *Nat. Cancer* **5**, 66–84 (2024).
34. Ikeuchi, K., Yazaki, E., Kudo, K. & Inada, T. Conserved functions of human Pelota in mRNA quality control of nonstop mRNA. *FEBS Lett.* **590**, 3254–3263 (2016).
35. Fogh, J., Fogh, J. M. & Orfeo, T. One hundred and twenty-seven cultured human tumor cell lines producing tumors in nude mice. *J. Natl. Cancer Inst.* **59**, 221–226 (1977).
36. Huvila, J. et al. Endometrial carcinosarcomas are almost exclusively of p53abn molecular subtype after exclusion of mimics. *Int. J. Gynecol. Pathol.* **43**, 506–514 (2024).
37. Zhu, X. et al. Alanine supplementation exploits glutamine dependency induced by SMARCA4/2-loss. *Nat. Commun.* **14**, 2894 (2023).
38. Tsuji, A., Akao, T., Masuya, T., Murai, M. & Miyoshi, H. IACS-010759, a potent inhibitor of glycolysis-deficient hypoxic tumor cells, inhibits mitochondrial respiratory complex I through a unique mechanism. *J. Biol. Chem.* **295**, 7481–7491 (2020).
39. Borck, P. C. et al. SKI complex loss renders 9p21.3-deleted or MSI-H cancers dependent on PELO. *Nature*, https://doi.org/10.1038/s41586-024-08509-3 (2025).
40. Pisareva, V. P., Skabkin, M. A., Hellen, C. U., Pestova, T. V. & Pisarev, A. V. Dissociation by Pelota, Hbs1 and ABCE1 of mammalian vacant 80S ribosomes and stalled elongation complexes. *EMBO J.* **30**, 1804–1817 (2011).
41. Zinoviev, A., Ayupov, R. K., Abaeva, I. S., Hellen, C. U. T. & Pestova, T. V. Extraction of mRNA from stalled ribosomes by the Ski complex. *Mol. Cell* **77**, 1340–1349.e1346 (2020).
42. Falck, J., Petrini, J. H., Williams, B. R., Lukas, J. & Bartek, J. The DNA damage-dependent intra-S phase checkpoint is regulated by parallel pathways. *Nat. Genet.* **30**, 290–294 (2002).
43. Myers, J. S., Zhao, R., Xu, X., Ham, A. J. & Cortez, D. Cyclin-dependent kinase 2 dependent phosphorylation of ATRIP regulates the G2-M checkpoint response to DNA damage. *Cancer Res.* **67**, 6685–6690 (2007).
44. Chung, J. H. & Bunz, F. Cdk2 is required for p53-independent G2/M checkpoint control. *PLoS Genet.* **6**, e1000863 (2010).
45. Zalzali, H. et al. CDK2 transcriptional repression is an essential effector in p53-dependent cellular senescence-implications for therapeutic intervention. *Mol. Cancer Res.* **13**, 29–40 (2015).
46. Brown, V. E. et al. CDK2 regulates collapsed replication fork repair in CCNE1-amplified ovarian cancer cells via homologous recombination. *NAR Cancer* **5**, zcad039 (2023).
47. Stumpff, J., von Dassow, G., Wagenbach, M., Asbury, C. & Wordeman, L. The kinesin-8 motor Kif18A suppresses kinetochore movements to control mitotic chromosome alignment. *Dev. Cell* **14**, 252–262 (2008).
48. Quinton, R. J. et al. Whole-genome doubling confers unique genetic vulnerabilities on tumour cells. *Nature* **590**, 492–497 (2021).
49. Marquis, C. et al. Chromosomally unstable tumor cells specifically require KIF18A for proliferation. *Nat. Commun.* **12**, 1213 (2021).
50. Cohen-Sharir, Y. et al. Aneuploidy renders cancer cells vulnerable to mitotic checkpoint inhibition. *Nature* **590**, 486–491 (2021).
51. Wong, N. K. Y. et al. Establishment and validation of preclinical models of SMARCA4-inactivated and ARID1A/ARID1B co-inactivated dedifferentiated endometrial carcinoma. *Gynecol. Oncol.* **176**, 162–172 (2023).
52. Yap, T. A. et al. Complex I inhibitor of oxidative phosphorylation in advanced solid tumors and acute myeloid leukemia: phase I trials. *Nat. Med.* **29**, 115–126 (2023).
53. Villafranca-Magdalena, B. et al. Genomic validation of endometrial cancer patient-derived xenograft models as a preclinical tool. *Int. J. Mol. Sc.* **23**, https://doi.org/10.3390/ijms23116266 (2022).
54. Gao, Y., Liu, T., Cheng, W. & Wang, H. Isolation and characterization of proliferative, migratory and multidrug-resistant endometrial carcinoma-initiating cells from human type II endometrial carcinoma cell lines. *Oncol. Rep.* **28**, 527–532 (2012).

55. Theisen, E. R. et al. Reversible inhibition of lysine specific demethylase 1 is a novel anti-tumor strategy for poorly differentiated endometrial carcinoma. *BMC Cancer* **14**, 752 (2014).
56. Wang, Y. et al. Ellagic acid exerts antitumor effects via the PI3K signaling pathway in endometrial cancer. *J. Cancer* **10**, 3303–3314 (2019).
57. Landrum, M. J. et al. ClinVar: public archive of relationships among sequence variation and human phenotype. *Nucleic Acids Res.* **42**, D980–D985 (2014).
58. Chen, S. et al. A genomic mutational constraint map using variation in 76,156 human genomes. *Nature* **625**, 92–100 (2024).
59. Sanjana, N. E., Shalem, O. & Zhang, F. Improved vectors and genome-wide libraries for CRISPR screening. *Nat. Methods* **11**, 783–784 (2014).

Acknowledgements

We thank Ms. Clara Salamanca, Ms. Emma Guo and all staffs from the Molecular and Advanced Pathology Core at the University of British Columbia for technical support. This work was supported by research funds from the Canadian Institutes of Health Research (CIHR) grants (PJT-178179; PJT-197923, to Y.W.), Terry Fox New Frontiers Program Project Grants (TFRI PPG, #1116, to L.H., Y.W. and D.G.H.) and Natural Science and Engineering Research Council-discovery grant (RGPIN-2020-05390, to R.I.K.G.). R.H., B.Y., and L.J. are recipients of the Canadian Graduate Scholarships-Master's Program. R.H. is a recipient of the Canadian Cancer Society Training Research Training Award. We also appreciate the generous support from the British Columbia Cancer Foundation and the VGH/UBC Hospital Foundation to the Ovarian Cancer Research Centre. The funder played no role in study design, data collection, analysis, and interpretation of data, or the writing of this manuscript.

Author contributions

E.L. and R.H.: investigation, data analysis, manuscript writing-first draft and editing; R.T. and C.Y.S.: investigation and manuscript editing; Y.W.Y.C., S.Y.C., J.S., B.Y., L.J., E.Y., and S.D.M.: investigation; M.C. and B.T.H.: resource; D.G.H. and R.I.K.G.: funding acquisition and supervision; L.H.: funding acquisition, investigation, and supervision; and Y.W.: conceptualization, supervision, funding acquisition, manuscript writing-first draft and editing. All authors read and approve the final version of the manuscript.

Competing interests

The authors declare no competing interests.

Additional information

Supplementary information The online version contains supplementary material available at https://doi.org/10.1038/s41698-025-01053-x.

Correspondence and requests for materials should be addressed to Yemin Wang.